Medicinal Chemistry Research (2020) 29:1247–1263
https://doi.org/10.1007/s00044-020-02581-w

MEDICINAL CHEMISTRY RESEARCH

ORIGINAL RESEARCH

Dioxin-like and non-dioxin-like PCBs differentially regulate the hepatic proteome and modify diet-induced nonalcoholic fatty liver disease severity

Jian Jin[1] · Banrida Wahlang[2,3] · Hongxue Shi[1,4] · Josiah E. Hardesty[2] · K. Cameron Falkner[2] · Kimberly Z. Head[2] · Sudhir Srivastava[5,6] · Michael L. Merchant[3,7] · Shesh N. Rai[3,5] · Matthew C. Cave[1,2,3,8,9] · Russell A. Prough[8]

Received: 15 April 2020 / Accepted: 30 May 2020 / Published online: 7 June 2020

Abstract

Polychlorinated biphenyls (PCBs) are persistent organic pollutants associated with metabolic disruption and nonalcoholic fatty liver disease (NAFLD). Based on their ability to activate the aryl hydrocarbon receptor (AhR), PCBs are subdivided into two classes: dioxin-like (DL) and non-dioxin-like (NDL) PCBs. Previously, we demonstrated that NDL PCBs compromised the liver to promote more severe diet-induced NAFLD. Here, the hepatic effects and potential mechanisms (by untargeted liver proteomics) of DL PCBs and NDL PCBs or co-exposure to both in diet-induced NAFLD are investigated. Male C57Bl/6 mice were fed a 42% fat diet and exposed to vehicle control; Aroclor1260 (20 mg/kg, NDL PCB mixture); PCB126 (20 μg/kg, DL PCB congener); or a mixture of Aroclor1260 (20 mg/kg) + PCB126 (20 μg/kg) for 12 weeks. Each exposure was associated with a distinct hepatic proteome. Phenotypic and proteomic analyses revealed increased hepatic inflammation and phosphoprotein signaling disruption by Aroclor1260. PCB126 decreased hepatic inflammation and fibrosis at the molecular level; while altering cytoskeletal remodeling, metal homeostasis, and intermediary/xenobiotic metabolism. PCB126 attenuated Aroclor1260-induced hepatic inflammation but increased hepatic free fatty acids in the co-exposure group. Aroclor1260 + PCB126 exposure was strongly associated with multiple epigenetic processes, and these could potentially explain the observed nonadditive effects of the exposures on the hepatic proteome. Taken together, the results demonstrated that PCB exposures differentially regulated the hepatic proteome and the histologic severity of diet-induced NAFLD. Future research is warranted to determine the AhR-dependence of the observed effects including metal homeostasis and the epigenetic regulation of gene expression.

Keywords PCBs · Aroclor1260 · PCB126 · Proteomics · NAFLD · TASH

Abbreviations

ACHS	Anniston Community Health Survey
AhR	Aryl hydrocarbon receptor
AK3L1	Adenylate kinase isoenzyme
Alb	Albumin

These authors contributed equally: Jian Jin, Banrida Wahlang

Supplementary information The online version of this article (https://doi.org/10.1007/s00044-020-02581-w) contains supplementary material, which is available to authorized users.

✉ Russell A. Prough
russell.prough@louisville.edu

[1] Department of Pharmacology & Toxicology, School of Medicine, University of Louisville, Louisville, KY 40202, USA

[2] Division of Gastroenterology, Hepatology, and Nutrition, Department of Medicine, School of Medicine, University of Louisville, Louisville, KY 40202, USA

[3] UofL Superfund Research Center, University of Louisville, Louisville, KY 40202, USA

[4] Department of Medicine, Columbia University Irving Medical Center, New York, NY 10032, USA

[5] Department of Bioinformatics and Biostatistics, School of Public Health and Information Sciences, University of Louisville, Louisville, KY 40202, USA

[6] Centre for Agricultural Bioinformatics, ICAR-Indian Agricultural Statistics Research Institute, New Delhi 110012, India

[7] Division of Nephrology and Hypertension, School of Medicine, University of Louisville, Louisville, KY 40202, USA

[8] Department of Biochemistry & Molecular Genetics, School of Medicine, University of Louisville, Louisville, KY 40202, USA

[9] Robley Rex Veterans Affairs Medical Center, Louisville, KY 40206, USA

ALT	Alanine transaminase
AML1	Acute myeloid leukemia 1
AST	Aspartate transaminase
BW	Body weight
CAE	Chloroacetate esterase
CAR	Constitutive androstane receptor
Cd68	Cluster of differentiation 68
c-FOS	Cellular oncogene FOS
Cyp	Cytochrome P450
DL	Dioxin-like
EGFR	Epidermal growth factor receptor
EPF	Enrichment by protein function
ERK	Extracellular signal-regulated kinases
ETS1	Protein C-ets-1
Fabp1	Fatty acid binding protein 1
Fasn	Fatty acid synthase
GABPα	GA binding protein transcription factor subunit α
GCR	Glucocorticoid receptor
GO	Gene ontology
H&E	Hematoxylin–eosin
HFD	High-fat diet
IPF	Interaction by protein function
KNG1	Kininogen 1
LW	Liver weight
mTOR	Mammalian target of rapamycin
NAFLD	Nonalcoholic fatty liver disease
NASH	Nonalcoholic steatohepatitis
NDL	Non-dioxin-like
NHANES	National Health and Nutrition Examination Survey
N-Myc	Neuroblastoma MYC oncogene
p38γ	Alternate mitogen-activated protein kinase
PCBs	Polychlorinated biphenyls
Pck1	Phosphoenolpyruvate carboxykinase 1
PKCα	Protein kinase C α
Pnpla3	Patatin-like phospholipase domain-containing protein 3
Ppara	Peroxisome proliferator-activated receptor alpha
Pparg	Peroxisome proliferator-activated receptor gamma
PRMT1	Protein arginine methyltransferase 1
PXR	Pregnane-xenobiotic receptor
SART1	Hypoxia-associated factor
Scd1	Stearoyl-CoA desaturase-1
SOX17	SRY-box transcription factor 17
Srebf1	Sterol regulatory element-binding protein 1
TASH	Toxicant-associated steatohepatitis
TCDD	Tetrachlorodibenzo-p-dioxin
TMT	Tandem mass tag
ZFPM1	Zinc finger protein
FOG	Family member 1
ZFX	Zinc finger protein x-linked

Introduction

The pollutants, polychlorinated biphenyls (PCBs), are metabolism-disrupting chemicals associated with nonalcoholic fatty liver disease (NAFLD), obesity, dyslipidemia, diabetes, and cardiovascular disease (Raffetti et al. 2018; Rosenbaum et al. 2017; Everett et al. 2011; Cave et al. 2010; Goncharov et al. 2008; Heindel et al. 2017). PCBs were produced during the 1930s–1970s for use in multiple industrial applications (Addison 1983). Although intentional PCB production is banned, their high thermodynamic stability imparting resistance to metabolism and degradation make PCBs persistent organic pollutants. PCBs bioaccumulate in living organisms and exposures increase along trophic levels of the food chain. PCBs have been detected in the serum of 100% American adult participants in the National Health and Nutrition Examination Survey (NHANES) (Cave et al. 2010).

The 209 possible PCB congeners have been generally categorized into two major classes: “coplanar” and “non-coplanar”. Coplanar PCBs (no or one chlorine atom in the ortho-position) including PCB126 potently activate the aryl hydrocarbon receptor (AhR), thereby eliciting a dioxin-like (DL) response similar to TCDD, and are known as “DL” PCBs (Safe et al. 1985). In contrast, noncoplanar PCBs have two or more chlorine atoms at the *ortho*-position, conferring a conformation that precludes AhR binding and activation. However, these so-called “non-DL” (NDL) PCBs activate other xenobiotic receptors, such as the constitutive androstane receptor (CAR) and elicit a phenobarbital-like response (Safe et al. 1985). Commercially, PCBs were sold as mixtures rather than individual congeners. Arclor1260 (60% chlorine by weight) was a first-generation PCB mixture manufactured in Anniston Alabama, by Monsanto. The Anniston Community Health Survey I reported a high prevalence of suspected NAFLD associated with PCB congener exposures in Anniston residents (Clair et al. 2018). The PCB congeners that constitute Aroclor1260 are ones that have higher molecular weights and are not easily metabolized; therefore, they tend to bioaccumulate in living organisms including humans. In fact, the PCB composition in Aroclor1260 more closely resembles human bioaccumulation patterns than any other single commercially produced Aroclor mixture (Wahlang et al. 2014a). Because low-dose Aroclor1260 does not activate either the human or murine AhR, Aroclor1260 has previously been used to model NDL PCB exposures (Wahlang et al. 2014a, b, 2016).

PCB exposures are associated with NAFLD in human cohort studies and either cause or exacerbate diet-induced NAFLD in animal studies (reviewed in (Wahlang et al. 2019a)). NAFLD is a broad spectrum of progressive liver disorders ranging from fat accumulation (steatosis) to

hepatic inflammation (steatohepatitis), fibrosis, cirrhosis, and hepatocellular carcinoma. NAFLD and its more severe form, nonalcoholic steatohepatitis (NASH), can be due to various etiological factors, such as high-caloric intake, lifestyle habits, and more recently, environmental chemical exposures. Our group coined the term "toxicant-associated steatohepatitis" (TASH) to reflect the steatohepatitis associated with industrial chemical exposures (Wahlang et al. 2019b). However, recent studies have implicated known PCB receptors such as the AhR, CAR, pregnane-xenobiotic receptor (PXR), and epidermal growth factor receptor (EGFR) in PCB-induced TASH (Wahlang et al. 2019a).

In the liver, AhR activation by TCDD and PCB126 increased lipid accumulation and led to simple steatosis in short-term, rodent studies (Angrish et al. 2012; Hardesty et al. 2019b). CAR, along with PXR, function as sensors of xenobiotic substances and are primarily involved in detoxification and foreign compound metabolism. However, previous studies from our group and others have shown that NDL PCB-mediated CAR and PXR activation also play a fundamental role in regulating hepatic energy metabolism and may contribute to TASH development (Wahlang et al. 2019a). Like phenobarbital, some PCBs appear to indirectly activate CAR by diminishing EGFR phosphorylation, leading to reduced hepatic phosphoprotein signaling and metabolic disruption in TASH (Hardesty et al. 2017, 2019a, b). Nonetheless, these studies only evaluated the effects of either DL or NDL PCBs in diet-induced obesity, although both classes of PCBs are concurrently present in the human exposome. We recently developed a new PCB exposure model, by spiking the potent AhR agonist, PCB126, into Aroclor1260 (Hardesty et al. 2019b). This mixture produced different hepatic effects than either Aroclor1260 or PCB126 alone in an acute exposure model (Hardesty et al. 2019b). Therefore, the objective of the current study is to evaluate the modulation of diet-induced NAFLD by several different types of chronic PCB exposures. Similar to our previous model (Hardesty et al. 2019b), these exposures include low-dose Aroclor1260 (representative NDL PCB mixture), PCB126 (prototypical DL PCB), and Aroclor1260 + PCB126 (NDL + DL PCB mixture). Untargeted liver proteomics was performed to elucidate potential mechanisms for observed differences in NAFLD disease severity.

Materials and methods

Animal studies

The related animal protocol was ratified by the University of Louisville Institutional Animal Care and Use Committee. Adult male C57BL/6 mice (8 weeks old) were purchased from Jackson Laboratory and distributed into four equal groups ($n = 10$). All mice were fed a high-fat diet (HFD, 15.2, 42.7, and 42.0% of total calories from protein, carbohydrate, and fat, respectively, TekLad TD88137) throughout the study period. At 10 weeks of age, ten mice in each group were given either corn oil, Aroclor1260 (20 mg/kg), PCB126 (20 µg/kg), or a mixture of Aroclor1260 (20 mg/kg) plus 0.1% PCB126 (20 µg/kg) via a one-time gavage and followed for 12 weeks (Supplementary Fig. 1). At week 8 post gavage, a glucose tolerance test (GTT) was performed as described previously (Wahlang et al. 2019c). Dual energy X-ray absorptiometry (DEXA) scanning (Lunar PIXImus densitometer, WI) was performed to measure body fat composition before euthanasia. Whole blood for plasma, liver, and fat tissue samples was harvested after euthanasia.

Definition of PCB doses utilized

The doses of the different PCBs used in the present study were similar to those used in the acute study (Shi et al. 2019) and were designed to mimic doses relevant to human exposures. For example, Aroclor1260 at 20 mg/kg was designed to reflect serum PCB levels measured in the highest exposed quartile of the ACHS cohort (Silverstone et al. 2012), while PCB126 at 20 µg/kg (0.1% of Aroclor1260) was designed to mimic the percent of serum PCB126 measured in NHANES 2003–2004, relative to other heavily bioaccumulated PCBs such as PCB153, the congener with the highest reported serum levels in NHANES 2003–2004 (Serdar et al. 2014).

Histological staining

Liver and pancreas tissues were fixed in 10% neutral buffered formalin for 72 h and embedded in paraffin for routine histological examination. Hematoxylin–eosin (H&E) staining was performed to identify histopathological changes. Chloroacetate esterase (CAE) activity, macrophage accumulation, and fibrosis were evaluated by CAE, immunohistochemical staining, and picro sirius red staining, respectively, according to the manufacturer's protocols. Micrographic images were obtained by a high-resolution Olympus digital scanner with an Olympus digital camera (BX41).

Real-time PCR

Mouse liver and pancreas tissues were homogenized and total RNA was extracted using RNA-STAT 60 reagent according to the manufacturer's protocol. The purity and quantity of total RNA were measured with a Nanodrop spectrometer (ND-1000, Thermo Fisher Scientific, Wilmington, DE) using ND-1000 V3.8.1 software and cDNA

was reverse transcribed from 1 µg RNA using a one-step cDNA synthesis reagent (QScript cDNA Supermix, QuantaBio, Beverly, MA). RT-PCR was performed on the CFX384^{TM} Real-Time System (Bio-Rad, Hercules, CA) using iTaq Universal Probe Supermix and Taqman probes as described elsewhere (Wahlang et al. 2019c). The relative mRNA expression was calculated using the comparative $2^{-\Delta\Delta Ct}$ method and normalized against GAPDH mRNA.

Measurement of hepatic lipids, plasma lipids, and cytokines

Hepatic lipids were extracted by a mixture of chloroform and methanol (2:1) according to a published protocol (Bligh and Dyer 1959). Triglycerides and free fatty acid contents were measured using commercial kits with final values normalized to liver weight. Plasma alanine transaminase (ALT), aspartate transaminase (AST), triglyceride, cholesterol, and lipoproteins were quantified with lipid panel plus kits on a Piccolo Xpress Chemistry Analyzer (Abbott Laboratories, IL). Plasma cytokine and adipokine levels were acquired using a customized Milliplex® MAP mouse adipokine panel on a Luminex® 100 system (Luminex Corp, Austin, TX).

Proteomics analysis

Proteins were extracted from liver tissue in RIPA buffer supplemented with protease and phosphatase inhibitors using a bead homogenizer and protein amounts were quantitated by BCA assay. Protein lysates (200 µg) were trypsinized using the modified filter-aided sample preparation method (Wisniewski et al. 2009) and enriched for phosphopeptides by the TiO2–SIMAC–HILIC method (Engholm-Keller and Larsen 2016). Briefly, protein samples were reduced with dithiothreitol, denatured with 8 M urea, and alkylated with iodoacetamide followed by centrifugation through a high molecular weight cutoff centrifugal filter (Millipore, 10k MWCO). After overnight digestion with sequencing grade trypsin (Promega), the digested proteins were collected and cleaned with a C18 Proto™ 300 Å Ultra MicroSpin column. Protein digested samples (50 µg) were labeled with tandem mass tag (TMT) TMT10plex™ Isobaric Label Reagent Set (Thermo Fisher, Waltham, MA); samples were then concentrated and desalted with Oasis HLB Extraction cartridges (Waters Corporation, Milford, MA) using a modified protocol for extraction of the digested peptides. (Keshishian et al. 2015). Samples were then subjected to high pH reversed phase separation with fraction concatenation on a Beckman System Gold LC system supplemented with 126 solvent module and 166 detector in tandem with a Bio-Rad Model 2110 Fraction Collector (McDowell et al. 2013). Liquid chromatography/mass spectrometry was used to measure TMT-labeled peptides. Briefly, every high pH reversed phase fraction was dissolved in 50 µL solution of the combination of 2% v/v acetonitrile/0.1% v/v formic acid and 1 µL of each fraction was analyzed on EASY-nLC 1000 UHPLC system (Thermo Fisher) and an Orbitrap Elite—ETD mass spectrometer (Thermo Fisher Scientific, Waltham, MA, USA). Proteome Discoverer v2.2.0.388 was used to analyze the raw data collected from the mass spectrometer. Hepatic proteins that had significance abundance were imported into MetaCore software (Clarivate Analytics, Philadelphia, PA) for the following analyses: gene ontology (GO), enrichment by protein function (EPF), and interaction by protein function (IPF).

Statistical analysis and data sharing

Statistical significance was determined by two-way analysis of variance using GraphPad Prism version 7.02 for Windows (GraphPad Software Inc., La Jolla, CA, USA). $p < 0.05$ was considered statistically significant. Statistical analysis for the proteome data was analyzed using the R package as described previously (Srivastava 2019a, b, c). Given the exploratory nature of the study, significantly altered proteins were further filtered using an FDR threshold of 0.2 and proteins exhibiting a fold change of $-0.5 < \log_2 FC < 0.5$ were rejected to rule out false positives. Proteomics data files were deposited with MassIVE (http://massive.ucsd.edu/) data repository, Center for Computational Mass Spectrometry at the University of California, San Diego, and shared with the ProteomeXchange (www.proteomexchange.org).

Results

Effects of PCB exposures on body composition, glucose tolerance, and adipokines

Body weight was measured weekly throughout the 12-week study. There was a gradual increase in body weight in all the four groups from week 0 to week 12 (Fig. 1a). However, there were no significant differences in the amount of body weight gain between the groups (Fig. 1b). Body fat composition was measured using both DEXA scan and by weighing the harvested epididymal fat (white adipose tissue) content. Although there was no significant difference in overall percent fat composition (Supplementary Fig. 2), Aroclor1260 exposure, however, increased white adipose tissue to body weight ratio (Fig. 1c). In addition, neither Aroclor1260 nor PCB126 affected liver weight to body weight ratio (Fig. 1d) and pancreas weight to body weight ratio in these mice (Supplementary Fig. 2). A GTT was performed to examine PCB effects on glucose metabolism; there were no differences between groups for alteration in glucose uptake (Supplementary Fig. 2). PCB effects on plasma lipids and

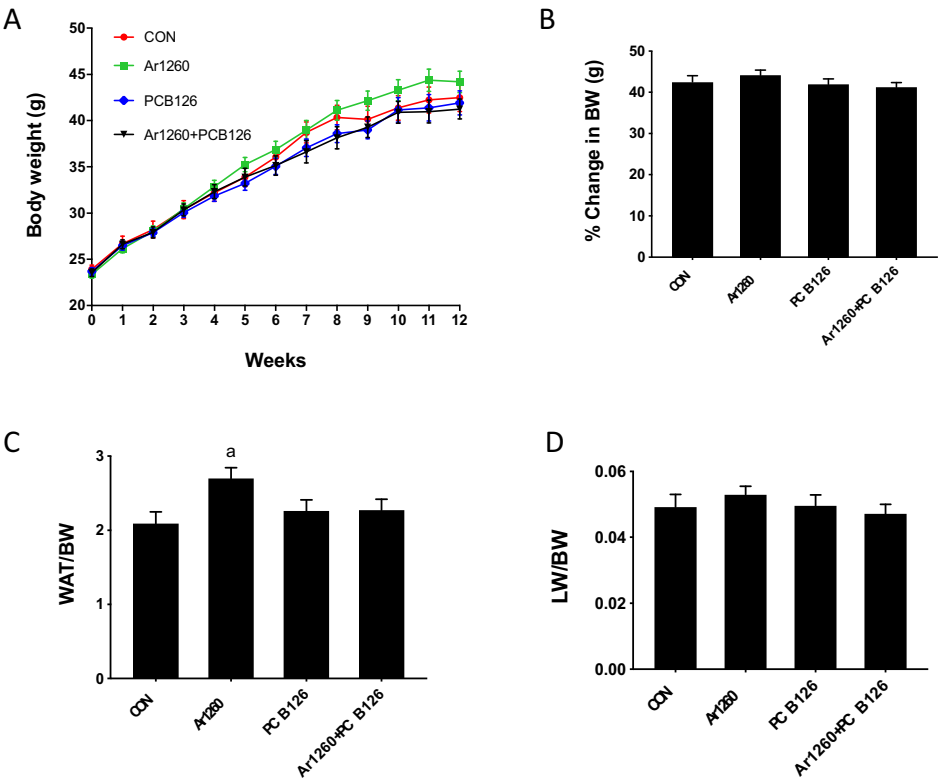

Fig. 1 Effects of PCB exposures on body composition. **a** Body weight (BW) was measured weekly throughout the 12-week study and **b** percent change in body weight relative to the initial body weight taken at the beginning of the study was calculated. White adipose tissue (WAT) weight and liver weight (LW) were measured and the **c** WAT/BW and **d** LW/BW ratios were calculated. Values are mean ± SEM; $p < 0.05$, **a**—Aroclor1260 effect, **b**—PCB126 effect, and **c**—interaction between Aroclor1260 and PCB126

adipocytokines were evaluated. The Aroclor1260 + PCB126 group significantly decreased plasma cholesterol levels via its interacting Aroclor1260 and PCB126 components. PCB126 exposure decreased triglyceride levels in the Aroclor1260 + PCB126 group (Supplementary Table 1). There was no PCB effect on adipokines including adiponectin, leptin, and resistin (Supplementary Table 1)

Effects of PCB exposure on hepatic steatosis, inflammation, injury, and fibrosis

Hepatic steatosis was assessed using H&E staining of liver sections. All HFD-fed mice developed variable, centrilobular, macrovesicular steatosis and the different PCB exposures did not exacerbate HFD-induced steatosis (Fig. 2a). Hepatic lipids were measured and PCB exposures had no effect on either hepatic triglyceride or cholesterol levels (Supplementary Fig. 3). However, hepatic free fatty acid levels were significantly increased by the Aroclor1260 + PCB126 mixture (Fig. 2b). Histological analyses for liver inflammation were assessed using CAE and F4/80 staining. CAE staining demonstrated that HFD feeding induced neutrophil infiltration in the liver (Fig. 2c); however, Aroclor1260 exposure exacerbated this effect as shown by the number of inflammatory foci counted per field (Fig. 2d). Interestingly, the Aroclor1260 + PCB126 group showed a lesser number of inflammatory foci counted per field. Likewise, F4/80 staining demonstrated that the Aroclor1260 group had increased macrophage infiltration compared with any other group (Fig. 2e). This observation was consistent with hepatic *Cd68* gene expression where in Aroclor1260 increased *Cd68* mRNA levels, indicating a hepatic inflammatory state, while this effect was absent with PCB126 exposure (Fig. 2f). Commonly used biomarkers of liver injury, namely plasma ALT and AST levels, were measured. Elevated plasma ALT activity levels were only seen with Aroclor1260 exposure, but not with PCB126 (Fig. 2g) while PCB126 showed a trend for decreased plasma AST activity levels (Supplementary Fig. 3). In addition, the Aroclor1260 + PCB126 group showed attenuation of Aroclor1260-elevated plasma ALT levels, suggesting that PCB126 may be protective against liver injury in this model. Fibrosis was assessed by picro sirius red staining of liver sections to detect collagen deposition (Supplementary Fig. 4). While there were no histological differences between groups, PCB126 decreased the hepatic gene expression of collagen (*Col1a2*) and actin 2 (*Acta2*), implicating a suppression of profibrotic gene expression in the liver (Supplementary Fig. 4)

PCB exposures modified expression of AhR and CAR target genes

Known PCB receptor activation such as AhR and CAR activation was examined. PCB126 exposure caused upregulation of cytochrome P450 1a2 (*Cyp1a2*), an AhR target

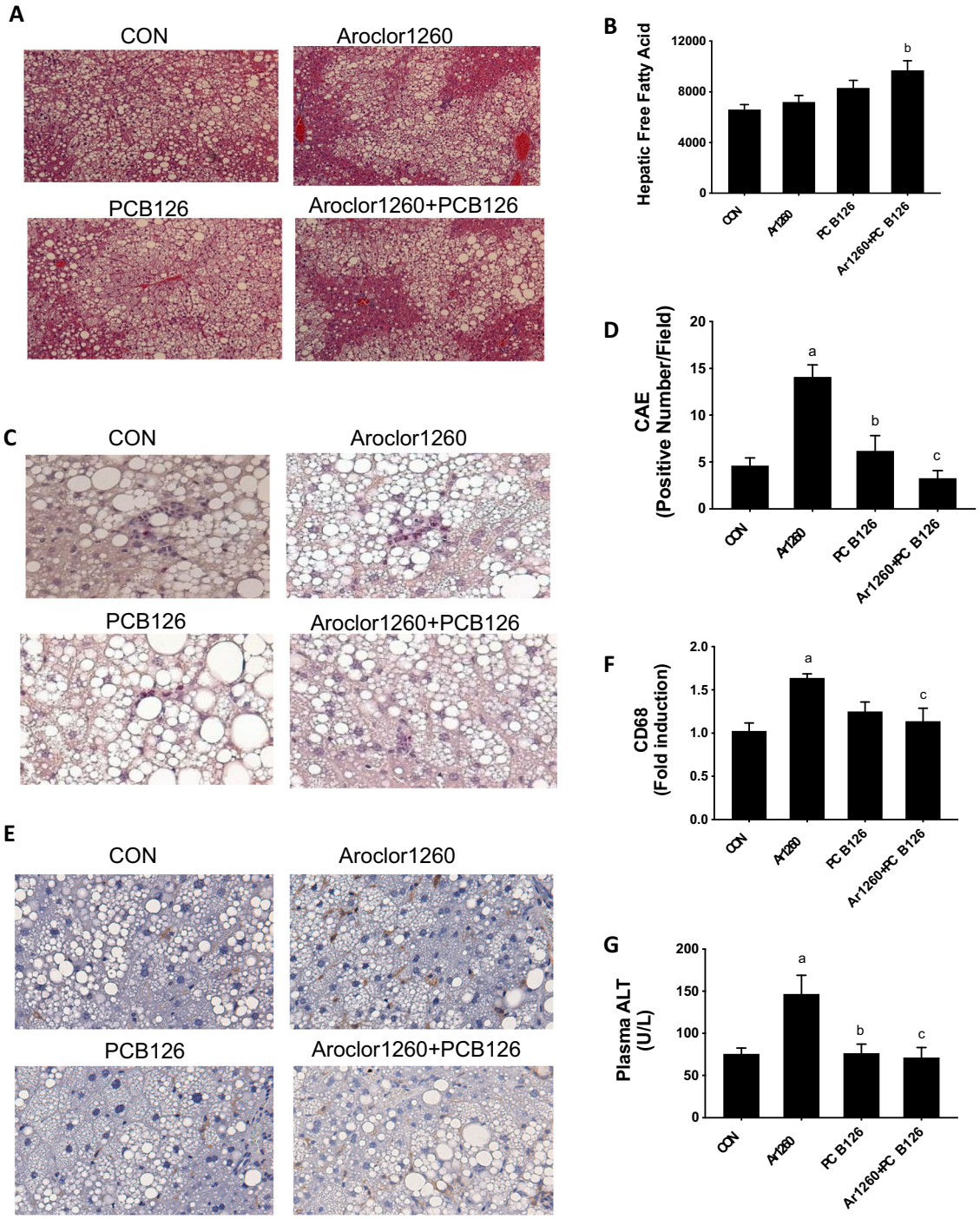

Fig. 2 Effects of PCB exposures on steatosis and inflammation. **a** Liver sections were analyzed for steatosis using H&E staining. **b** Hepatic free fatty acid levels were measured using colorimetric assay. **c** Liver sections were analyzed for neutrophil infiltration using CAE staining where red positive cells indicate neutrophil infiltration. **d** The CAE positive number per microscopic field was counted. **e** Liver sections were analyzed for macrophage infiltration using F4/80 immunohistochemistry staining and brown positive cells indicate macrophage accumulation. **f** Hepatic *CD68* mRNA levels were measured using RT-PCR. **g** Plasma ALT activity levels were measured using the Piccolo Xpress Chemistry Analyzer. Values are mean ± SEM; $p < 0.05$, **a**—Aroclor1260 effect, **b**—PCB126 effect, and **c**—interaction between Aroclor1260 and PCB126

gene, indicative of AhR activation. In contrast, the Aroclor1260 + PCB126 group showed decreased *Cyp1a2* mRNA levels (Fig. 3a). With regards to AhR gene expression, PCB126 alone showed a trend for decreased *AhR* mRNA levels (Fig. 3b). For CAR activation, the CAR target gene, *Cyp2b10*, was measured. The Aroclor1260

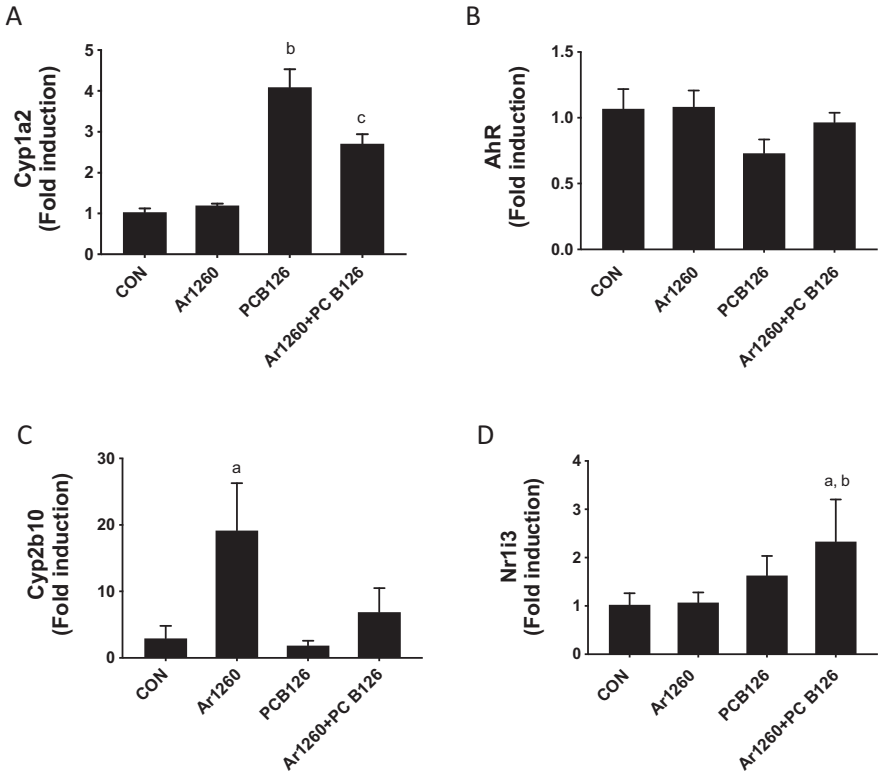

Fig. 3 Effects of PCB exposures on target gene expression. Hepatic mRNA expression for the AhR target gene **a** *Cyp1a2* and **b** *AhR* and the CAR target gene target gene *Cyp2b10* (**c**) and (**d**) CAR (*Nr1i3*) were measured by RT-PCR. Values are mean ± SEM; $p < 0.05$, **a**—Aroclor1260 effect, **b**—PCB126 effect, and **c**—interaction between Aroclor1260 and PCB126

group showed upregulated *Cyp2b10* mRNA levels, indicative of CAR activation (Fig. 3c), while CAR expression was increased in the Aroclor1260 + PCB126 groups (Fig. 3d).

Effects of PCB exposure on the hepatic proteome

The various PCB exposures produced distinct hepatic proteomes (Fig. 4). A total of 8355 unique proteins and their isoforms were detected, corresponding to 4609 protein groups. Liver protein content was regulated as follows: Aroclor1260 (35 increased and 48 decreased); PCB126 (158 increased and 238 decreased); and Aroclor1260 + PCB126 (144 increased and 257 decreased) (Fig. 4 and Supplementary Table 2). The majority of differentially abundant proteins for each group were unique to that exposure (range 58.7–63.1%). Of the 401 proteins associated with Aroclor1260 + PCB126 exposure, only 5.9% were also associated with Aroclor1260, while only 33.6% were also associated with PCB126. Only three proteins were changed in all three PCB exposure groups (BET1-like protein and two isoforms of protein-O-linked-mannose-β-1,4-N-acetylglucosaminyltransferase 2). Clearly, the proteomic changes associated with the Aroclor1260 + PCB126 mixture were not the sum of its parts.

EPF analysis was performed to determine the protein classes most impacted by PCBs (Supplementary Table 3). Enzymes were the most affected class (Aroclor1260, z-score = 3.63; PCB126, z-score = 7.11; Aroclor1260 + PCB126, z-score = 4.89). Consistent with this observation and the RT-PCR data, the enzyme levels of CYP1A1 and CYP1A2 were higher for PCB126 (CYP1A1: 9.09-fold, $p = 7.10\text{E}{-06}$ and CYP1A2: 5.85-fold, $p = 3.10\text{E}{-08}$) and, to a lesser degree, for Aroclor1260 + PCB126 (CYP1A2: 2.39-fold, $p = 2.39\text{E}{-08}$) (Supplementary Table 2). While Aroclor1260 increased hepatocyte injury (by histologic and plasma ALT enzyme activity biomarkers), plasma AST activity was not significantly increased. This could be related to the peculiar proteomic observation that hepatic AST enzyme levels were reduced by PCB exposures (Aroclor1260: 0.64-fold, $p = 2.18\text{E}{-03}$ and PCB126 0.68-fold, $p = 5.82\text{E}{-03}$). Again, consistent with the liver histology, inflammation-associated enzymes and leukocyte markers were increased with Aroclor1260 (e.g., macrosialin/CD68, 2.26-fold, $p = 1.85\text{E}{-04}$) and decreased with either PCB126 (e.g., myeloperoxidase: 0.51-fold, $p = 1.79\text{E}{-03}$; α-defensin 20: 0.48-fold, $p = 2.90\text{E}{-02}$; and the calprotectin component, protein S100-A8: 0.32-fold, $p = 8.05\text{E}{-03}$) or Aroclor1260 + PCB126 (e.g., protein S100-A9: 0.62-fold, $p = 4.35\text{E}{-02}$; neutrophil granule protein: 0.58-fold, $p = 1.17\text{E}{-02}$; protein jagunal homolog 1: 0.33-fold, $p = 1.20\text{E}{-02}$; and neutrophil gelatinase-associated lipocalin (0.30-fold, $p = 2.41\text{E}{-02}$) (Supplementary Table 2). EPF revealed that Aroclor1260 altered protein levels of slightly more transcription factors than expected (z-score = 1.67), while the other exposures changed fewer than expected. Several nuclear receptors implicated in

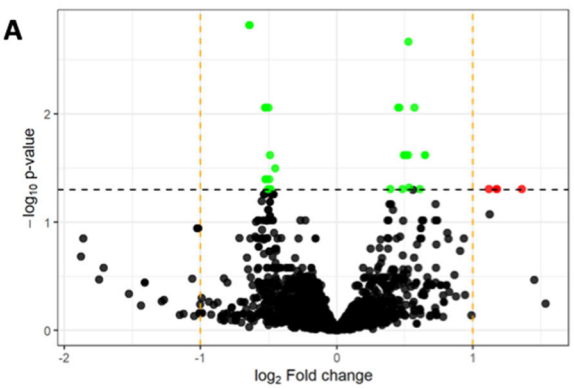

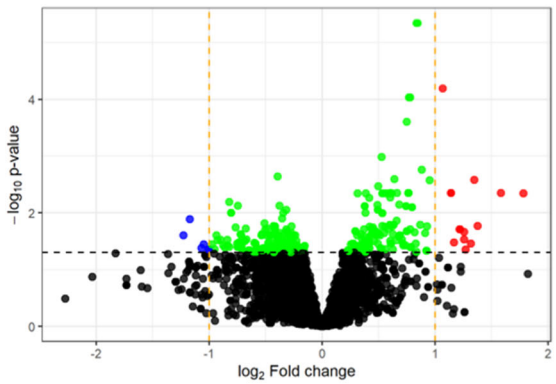

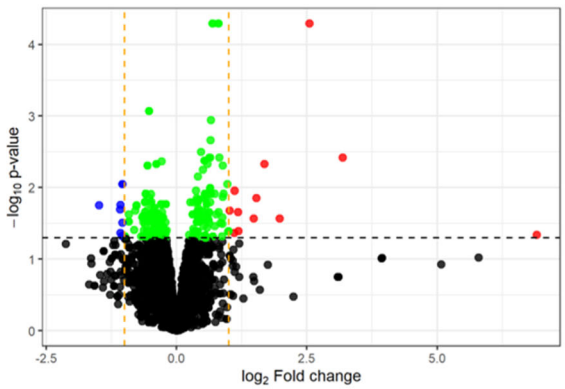

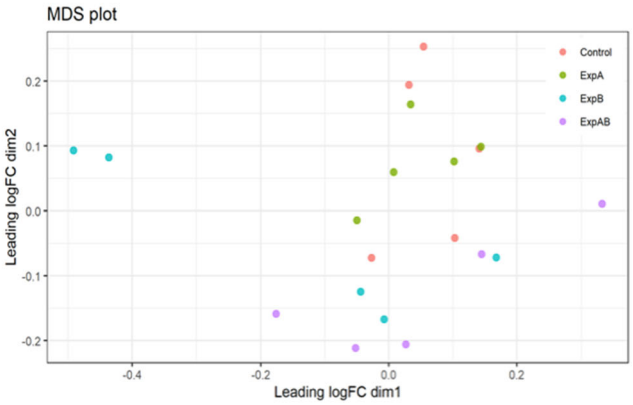

E

Adjusted (FDR=0.2)	Ar1260	PCB126	PCB126+ Ar1260
Altered	143	1663	1740
Increase ($log_2FC \geq 0.5$)	35	158	144
Decrease ($log_2FC \leq -0.5$)	48	238	257

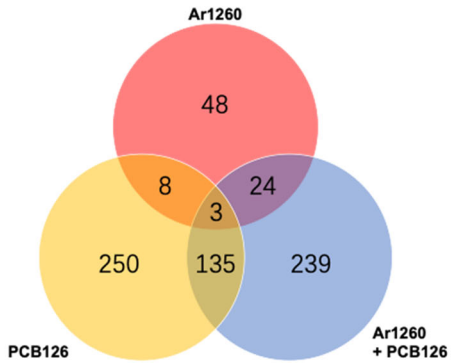

Fig. 4 Effects of PCB exposures on the hepatic proteome. Alterations in hepatic proteins are depicted by volcano plots showing significance (*y*-axis) versus protein fold change (*x*-axis) for **a** Aroclor1260, **b** PCB126, and **c** Aroclor1260 + PCB126. Black denotes unaltered proteins, green denotes significantly altered proteins, red denotes significantly altered protein with ($log_2FC > 1$), and blue denotes significantly altered protein with ($log_2FC < 1$). **d** A multidimensional scatter (MDS) plot depicting the pattern for protein alterations in the different groups. ExpA—Aroclor1260, ExpB—PCB126, and ExpC—Aroclor1260 + PCB126. **e** The number of proteins and their isoforms that were altered for the different exposure groups. **f** Venn diagram showing the number of overlapping proteins between the three exposure groups

steatohepatitis were differentially regulated including peroxisome proliferator-activated receptor alpha (PPARα, Aroclor1260: 0.7-fold, $p = 1.97E{-}03$), liver X receptor alpha (PCB126: 1.47-fold, $p = 1.81E{-}02$), and V-erbA-related protein 2 (PCB126: 0.69-fold, $p = 1.14E{-}02$ and Aroclor1260 + PCB126: 0.63-fold, $p = 2.69E{-}03$). Thus, while each PCB exposure was associated with a distinct proteome, EPF demonstrated that these proteomes were consistent with the observed phenotypes.

Enrichment by GO processes (Fig. 5) revealed that the distinct proteomes associated with PCB126 and Aroclor1260 + PCB126 exposures were associated with similar top GO processes, although some differences were apparent. However, the top GO processes associated with Aroclor1260 were unique to that exposure. These findings are again consistent with the histology and phenotyping data. A very limited number of GO processes were enriched by Aroclor1260 including "negative regulation of receptor

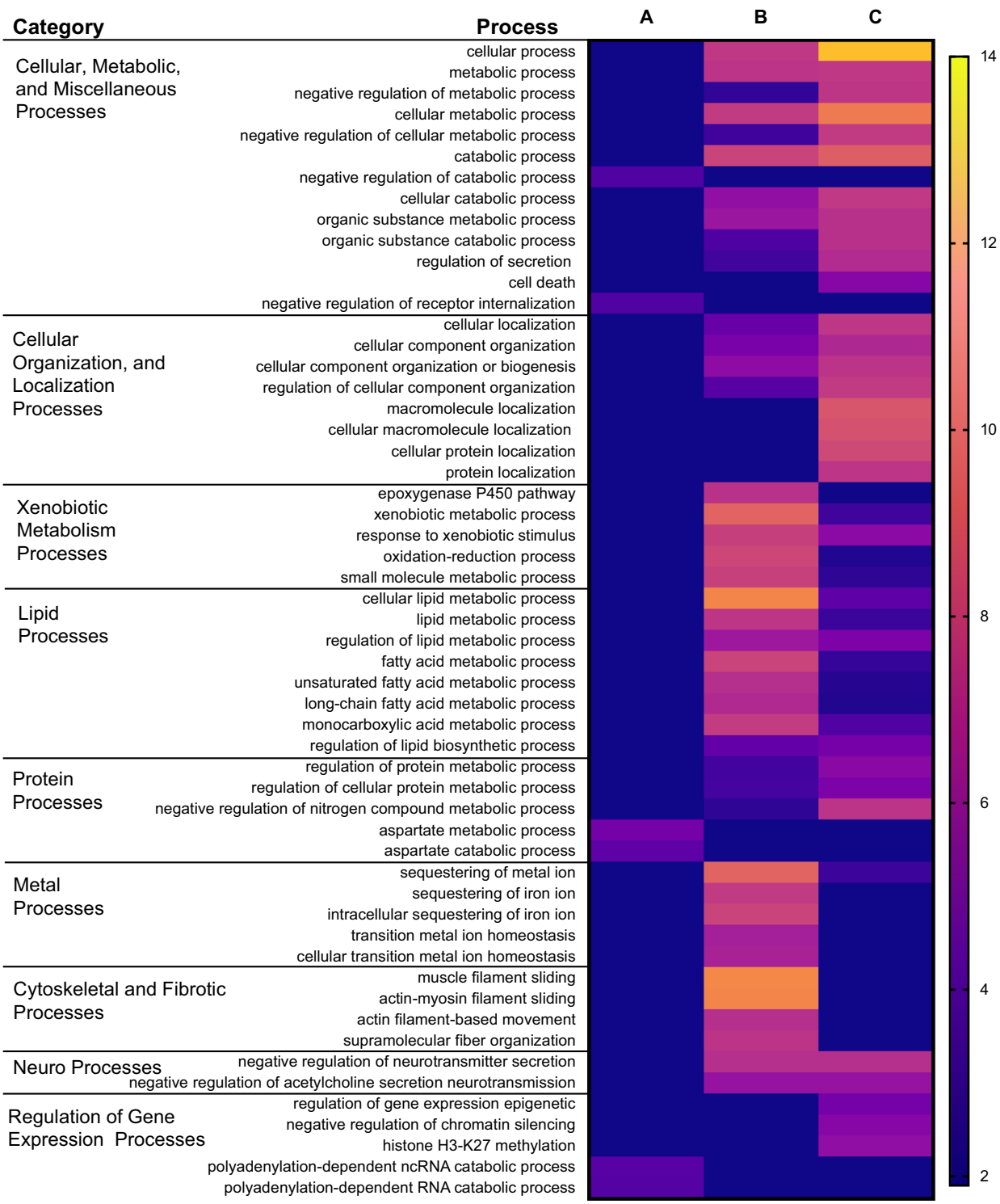

Fig. 5 PCB effects on gene ontology (GO) processes. Heatmap showing different processes that were altered by PCB exposures according to the $-\log(p\text{-value})$. The processes were obtained by GO analysis enrichment of the different proteins altered by PCB exposures using MetaCore. **a**—Aroclor1260, **b**—PCB126, **c**—Aroclor1260 + PCB126

internalization"; "negative regulation of catabolic process"; aspartate catabolic metabolism; and polyadenylation-dependent RNA catabolic processes (Fig. 5). In contrast, hundreds of GO processes were significantly enriched by PCB126 and/or Aroclor1260 + PCB126 (data not shown). Both exposures enriched: (i) cellular, metabolic, and catabolic processes; (ii) protein metabolism processes; (iii) cellular localization and organization processes; and (iv) the

"negative regulation of neurotransmitter (acetylcholine) secretion". These processes, however, were enriched to a greater degree by Aroclor1260 + PCB126. In contrast, while both exposures enriched xenobiotic metabolism processes and lipid metabolism processes, these were enriched to a greater degree by PCB126.

GO processes related to cytoskeletal remodeling/fibrosis and metal homeostasis were enriched by PCB126 only (Fig. 5). The abundance of several cytoskeletal-associated proteins were markedly increased by PCB126 including troponin C (120.33-fold, $p = 1.30E{-}03$); actin α, skeletal muscle (55.47-fold, $p = 7.38E{-}03$); myosin light chain 3 (33.67-fold, $p = 1.27E{-}02$); LIM domain-binding protein (15.24-fold, $p = 7.88E{-}03$), etc. (Supplementary Table 2). However, other cytoskeletal proteins, including type II keratins, were differentially regulated by Aroclor1260 (keratin 5: 0.28-fold, $p = 2.12E{-}03$) or Aroclor1260 + PCB126 (keratin 2: 0.30-fold, $p = 3.85E{-}02$; keratin 4: 0.62-fold, $p = 4.19E{-}02$; and keratin 6a: 1.89-fold, $p = 1.34E{-}02$). While the PCB exposures were not associated with fibrosis at the histologic level, PCB126 exposures were associated with reduced expression of several profibrogenic genes at the molecular level. Consistent with this observation, PCB126 was associated with reduced abundance of several proteins associated with liver fibrosis including collagen α-1(IV) chain (0.68-fold, $p = 2.26E{-}02$); prolyl 4-hydroxylase subunit alpha-1 (0.66-fold, $p = 1.42E{-}03$); and procollagen-lysine, 2-oxoglutarate 5-dioxygenase 3 (0.47-fold, $p = 2.28E{-}02$). Multiple proteins associated with metal homeostasis were likewise reduced only by PCB126 including ferritin light chain 1 (0.64-fold, $p = 1.44E{-}02$), light chain 2 (0.63-fold, $p = 1.24E{-}02$), and heavy chain (0.60-fold, $p = 6.11E{-}03$), and zinc transporter 4 (0.55-fold, $p = 3.09E{-}02$).

Several GO processes related to the epigenetic mechanisms were enriched only by Aroclor1260 + PCB126 (Fig. 5). These included "regulation of gene expression, epigenetic", "negative regulation of chromatin silencing", and "histone H3-K27 methylation". Differentially abundant proteins contributing to these observations included reduced histone deacetylase 2 (0.68-fold, $p = 1.13E{-}02$); reduced histones H1.2 (0.63-fold, $p = 5.98E{-}04$), H1.4 (0.66-fold, $p = 8.87E{-}03$), H1.5 (0.67-fold, $p = 2.45E{-}02$), and H1t (0.67-fold, $p = 1.40E{-}02$); reduced RNA polymerase-associated protein CTR9 homolog (0.60-fold, $p = 7.64E{-}04$); and reduced exportin 5 (0.66-fold, $p = 2.07E{-}02$). However, several other epigenetics proteins were reduced by PCB126 and Aroclor1260 + PCB126, such as RNA binding protein 3 (PCB126: 0.68-fold, $p = 2.64E{-}03$; Aroclor1260 + PCB126: 0.69-fold, $p = 2.78E{-}03$); LIM domain-containing protein 1 (PCB126: 0.66-fold, $p = 6.66E{-}03$; Aroclor1260 + PCB126: 0.63-fold, $p = 2.93E{-}03$); and protein arginine methyltransferase 7 (PCB126: 0.64-fold, $p = 9.69E{-}04$; Aroclor1260 + PCB126: 0.70-fold, $p = 4.74E{-}03$).

IPF analysis was performed and the top overconnected interactions by *z*-score are provided in Fig. 6. Seven unique objects, all protein kinases, were overconnected with Aroclor1260 exposure. These kinases included the mammalian target of rapamycin (mTOR); the adenylate kinase isoenzyme, mitochondrial (AK3L1); the alternate mitogen-activated protein kinase, p38γ; and protein kinase C α (PKCα). PCB126 and/or Aroclor1260 + PCB126 exposures were associated with 18 overconnected objects (Fig. 6). Eleven of these objects were transcription factors and eight of these were common between the two groups. Shared transcription factors included protein C-ets-1 (ETS1), SRY-box transcription factor 17 (SOX17), and GA binding protein transcription factor subunit α (GABPα); glucocorticoid receptor; zinc finger protein x-linked (ZFX); neuroblastoma MYC oncogene (N-Myc); and acute myeloid leukemia 1 (AML1). The *z*-scores were all higher with the Aroclor1260 + PCB126 exposure. Unique transcription factors overconnected by PCB126 included zinc finger protein, FOG family member 1 (ZFPM1), and CAR, while cellular oncogene FOS (c-FOS) was uniquely overconnected by Aroclor1260 + PCB126. PCB126 exposure was uniquely overconnected with the bradykinin precursor, kininogen 1, and thrombin. Aroclor1260 + PCB126 was uniquely overconnected with two enzymes associated with steatohepatitis and liver cancer, protein arginine methyltransferase 1 (PRMT1), and hypoxia-associated factor (SART1) (Zhao et al. 2019; Koh et al. 2016).

PCB effects on hepatic intermediary metabolism and plasma profile

Proteomics analysis revealed that PCBs played a role in dictating intermediary metabolism such as lipid and protein processes. To further validate these findings, hepatic expression of genes involved in a variety of metabolic processes, including lipogenesis, lipid transport and mobilization, fatty acid β-oxidation, and glucose and protein metabolism were measured. The expression of genes related to lipogenesis, namely, fatty acid synthase (*Fasn*), sterol regulatory element-binding protein 1 (*Srebf1*), stearoyl-CoA desaturase-1 (*Scd1*), and peroxisome proliferator-activated receptor gamma (*Pparg*) were measured by RT-PCR. PCB exposure did not alter *Fasn* or *Srebf1* mRNA levels although the PCB126 group demonstrated a trend for decreased *Fasn* and *Srebf1* mRNA levels (Supplementary Fig. 5), consistent with previous findings (Wahlang et al. 2017a, b). Similarly, Aroclor1260 + PCB126 exposure decreased *Scd1* mRNA levels (Fig. 7a), consistent with protein abundance data (0.70-fold, $p = 1.35E{-}02$, Supplementary Table 2) and a prior study (Hardesty et al. 2019b).

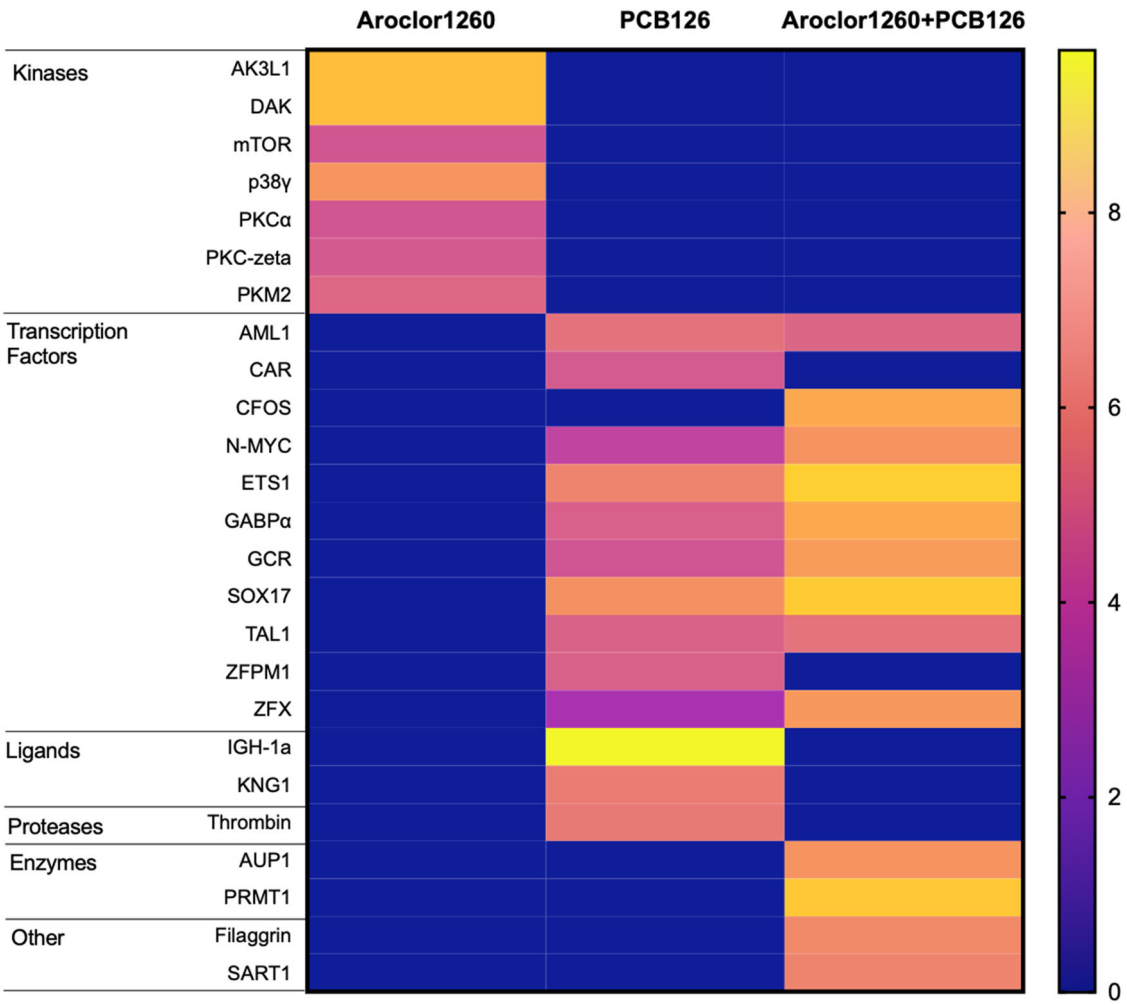

Fig. 6 Effects of PCB exposures on protein function. Heatmap showing different classes of proteins, for the three exposure groups, obtained from the Interaction by protein function analysis using MetaCore and their corresponding *z*-scores

The same group also showed increased *Pparg* gene expression (Fig. 7b). With regards to lipid transport, the hepatic mRNA levels of *Cd36* and fatty acid binding protein 1 (*Fabp1*) were determined. Both Aroclor1260 and PCB126 contributed to the upregulated *Cd36* expression in the Aroclor1260 + PCB126 mixture (Fig. 7c). There was no significant difference for *Fabp1* mRNA levels between groups (Supplementary Fig. 5). In terms of lipid breakdown, the mRNA levels of *Pparα*, a transcription factor that regulates fatty acid β-oxidation, the Aroclor1260 + PCB126 group decreased *Pparα* levels (Fig. 7d). These results differed from the proteomics data that showed decreased protein abundance only for Aroclor1260. PCB126 exposure also decreased the expression of the lipolytic gene, patatin-like phospholipase domain-containing protein 3 (*Pnpla3*, Fig. 7e). In addition, the gene expression of phosphoenolpyruvate carboxykinase 1 (*Pck1*), a gluconeogenic gene, was measured and found to be decreased with PCB126 exposure (Fig. 7f). Proteomics data demonstrated that PCB126 disrupted the coordination of glycolysis and gluconeogenesis by simultaneously downregulating abundance of hexokinase-3 (0.52-fold, $p = 2.53\text{E}{-}03$), phosphofructokinase (0.61-fold, $p = 6.53\text{E}{-}03$), and glucose-6-phosphatase (0.51-fold, $p = 1.33\text{E}{-}02$). The gene expression of albumin (*Alb*), a biomarker for protein metabolism, was increased in the Aroclor1260 + PCB126 group (Fig. 7g). Overall, these results confirm that PCBs differentially altered hepatic intermediary metabolic processes.

Discussion

PCBs, including both DL and NDL congeners, are metabolism-disrupting chemicals (Heindel et al. 2017). PCBs exposures are associated with obesity-related diseases including diabetes, dyslipidemia, cardiovascular disease, and NAFLD. PCB-related NAFLD mechanisms was

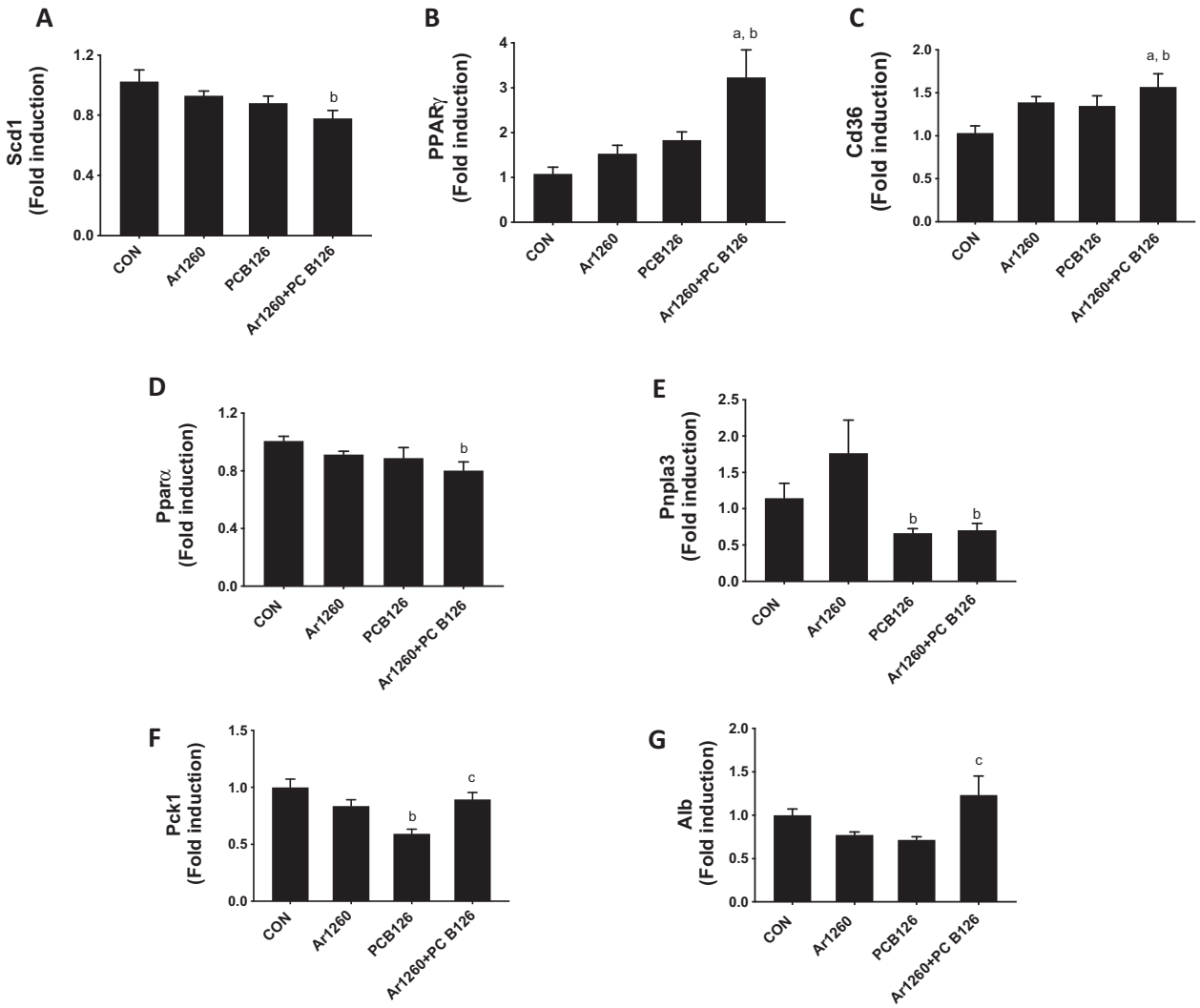

Fig. 7 Effects of PCB exposures on genes involved in hepatic energy metabolism. Hepatic mRNA levels of genes involved in hepatic energy metabolism including **a** *Scd1*, **b** *Pparg*, **c** *Cd36*, **d** *Pparα*, **e** *Pnpla3*, **f** *Pck1*, and **g** *Alb* were measured by RT-PCR. Values are mean ± SEM; $p < 0.05$, **a**—Aroclor1260 effect, **b**—PCB126 effect, and **c**—interaction between Aroclor1260 and PCB126

recently reviewed (Wahlang et al. 2019a). In animal models fed a healthy diet, DL, but not NDL PCBs, caused hepatic steatosis and NAFLD. In contrast, NDL PCBs exposures compromised the liver, thereby increasing the histologic severity of HFD-induced NAFLD. The NDL PCB exposures variably increased diet-induced hepatic steatosis, inflammation, and fibrosis while interacting with PCB receptors including PXR, CAR, and the EGFR (Wahlang et al. 2016, 2014b, 2019b; Hardesty et al. 2019b, 2017, 2019a, 2018). While humans have simultaneous exposures to both PCB classes, no previously published studies in the literature have systematically evaluated the disease modifying effects of DL PCBs, NDL PCBs, and the more environmentally relevant combination of DL + NDL PCBs in a chronic exposure model of HFD-induced NAFLD. Few to no published data exist on either DL or DL + NDL PCBs in such a model.

Our recently published acute PCB exposure study demonstrated that Aroclor1260, PCB126, and Aroclor1260 + PCB126 exposures differentially affected histology and disease mechanisms in liver and related organs in male mice fed a healthy diet (Shi et al. 2019). Based on the direction of these results, environmental relevance, and knowledge gaps in the literature, the objective of the current study was to elucidate the effects and potential mechanisms of these different PCB exposures in a diet-induced obesity mouse model of NAFLD.

The combination of the phenotyping, histologic, and molecular biomarkers demonstrated the following differential PCB effects on metabolic conditions related to HFD-induced obesity. Consistent with prior studies (Wahlang et al. 2019a), Aroclor1260 increased liver inflammation/injury and the white adipose tissue to body weight ratio. PCB126 decreased liver inflammation and fibrosis at the

molecular level. PCB126 alone did not increase hepatic free fatty acids and hepatic triglycerides, as reported previously (Shi et al. 2019). These differences are likely related to differences in duration of exposure or diet. Aroclor1260 + PCB126 modulated lipid metabolism such as hepatic free fatty acids were increased, while the plasma cholesterol/triglycerides were decreased, and it decreased liver inflammation. The lipid effects were mediated predominantly by the PCB126 component of this mixture as previously reported (Shi et al. 2019). Therefore, PCB126 co-exposure attenuated Aroclor1260-induced hepatic inflammation despite worsening the disruption of intermediary and xenobiotic metabolism. None of the exposures affected glucose tolerance or adipokines. AhR activation was highest with PCB126 alone; increased to a lesser degree with Aroclor1260 + PCB126; and absent with Aroclor1260, consistent with Shi et al. (2019). The effects on CAR were complex. *Cyp2b10* gene expression was increased by Ar1260; IPF demonstrated enriched CAR interactions with PCB126; and Aroclor1260 + PCB126 induced *Nr1i3* gene expression. PCBs induced *Cyp2b10* gene expression to a lower degree in HFD-fed mice compared with mice fed a low fat diet (Shi et al. 2019).

Proteomics was performed to elucidate potential mechanisms for the observed differences in metabolic phenotype and TASH severity, which were greatest for Aroclor1260 versus the more similar PCB126 and Aroclor1260 + PCB126 exposure groups. The large number of differentially abundant proteins between the PCB exposure groups was surprising. For example, 99.58% of these proteins were not conserved across all three treatment groups. PCB126 and Aroclor1260 + PCB126 altered many more proteins than Aroclor1260. However, 79.06% of the proteins altered by either of the latter two treatments were not common to both groups. Despite these differences, PCB126 and Arclor1260 + PCB126 shared many top GO processes consistent with the observed similarities in liver histologic phenotype. The observed alterations in cholinergic neurotransmission associated with these exposures is novel and could be mechanistic. For example, human neonates exposed to PCBs display a number of hematologic and immunologic disturbances in neuronal signaling, immune regulation via the AhR and other receptors (Patandin et al. 1998; ten Tusscher et al. 2003). In addition, these exposures alter many normal medical biomarkers used in clinical medicine, such as cholesterol levels, AST enzyme levels, etc.

While a number of new putative PCB targets and modes of action in TASH were identified, others were reassuringly consistent with known targets. Aroclor1260 exposure was associated with the "negative regulation of receptor internalization" GO process and overconnected interactions with protein kinases including mTOR, AK3L1, p38γ, and PKCα. These findings could be consistent with the decreased EGF-stimulated EGFR internalization with consequent phosphoprotein signaling disruption previously reported for Aroclor1260-associated TASH (Hardesty et al. 2017, 2019a, b, 2018; Wahlang et al. 2019c). These studies reported decreased protein kinase B (Akt)/mTOR and extracellular signal-regulated kinases (ERK) signaling. AK3L1 is a downstream EGFR target that regulates glycolysis, thereby adding a new link between signaling disruption and intermediary metabolism (Jan et al. 2019). Intriguingly, p38γ and PKCα regulate both EGF-dependent ERK signaling (Abera and Kazanietz 2015; Lei et al. 2017; Yin et al. 2017) and NASH (Gonzalez-Teran et al. 2016; Zhou et al. 2019). The potential mechanistic roles of these kinases warrant future investigation in Aroclor1260-associated TASH.

The observed alterations in GO processes related to hepatic metal hemostasis and cytoskeleton for PCB126 could be mechanistic. PCB126-induced metal dysregulation has been described previously (Klaren et al. 2015, 2018). However, the specific effector proteins identified by the present study (e.g., hepcidin, ferritin, zinc transporter 4, etc.) and the hepcidin-regulating transcription factor, ZFPM1, (Bagu et al. 2013) warrant future investigation. Several cytoskeleton proteins were the most upregulated proteins by PCB126. The other exposures were associated with altered abundance of keratins 2, 4, 5, or 6a. Cellular localization analysis of a previous hepatic proteomics experiment from our group demonstrated that cytoskeletal-associated proteins were the top enriched cellular location for liver proteins differentially regulated by Aroclor1260 in mice fed a control diet, but this decreased in HFD-fed mice (Hardesty et al. 2019b). Circulating epithelial cell-derived keratin18 was associated with PCB-related TASH in ACHS (Clair et al. 2018). Ethanol-associated alterations of the hepatocyte cytoskeleton may influence the progression of alcohol-related steatohepatitis (Shepard and Tuma 2010). Therefore, the potential mechanistic role of PCB-induced cytoskeletal changes in TASH warrants future investigation. If the observed reduction in hepatic AST protein abundance is confirmed in humans, the utility of circulating AST enzyme activity as a biomarker for PCB-related liver toxicity in environmental epidemiology studies would be reduced. Several GO processes uniquely enriched with Aroclor1260 + PCB126 co-exposure were discovered, including the epigenetic regulation of gene expression and the localization of macromolecules including proteins.

IPF analysis of the PCB126 and Aroclor1260 + PCB126 exposure groups revealed overconnected interactions with several transcription factors regulating myriad processes involved in the resolution and repair of liver injury including inflammation, stellate cell plasticity and fibrosis, stem cells, proliferation, differentiation, metabolism, and

transformation. These transcription factors are new targets for PCB hepatotoxicity in NASH and include ETS1 (Sizemore et al. 2017; Marcher et al. 2019), SOX17 (Rommelaere et al. 2014; Merino-Azpitarte et al. 2017), GABPα (Niopek et al. 2017; Sizemore et al. 2017), c-FOS (Bakiri et al. 2017), ZFX (Ding et al. 2018), N-Myc (Qin et al. 2018), and AML1 (Marcher et al. 2019). While tumors were not observed in the present study, the identification of oncogenes is not surprising because PCB126 has previously been associated with liver cancer. Although Cyp1a2 message and protein were induced by PCB126 and Aroclor1260 + PCB126, MetaCore analyses provided no evidence to support the potential AhR-dependence in any of the identified GO processes. Moreover, IPF analysis did not identify AhR as an overconnected transcription factor. While this could simply be a limitation of the software package, future studies are required to determine the AhR-dependence of PCB-related TASH.

Aroclor1260 and PCB126 did not result in either additive hepatotoxicity or additive differential protein abundances in this chronic, diet-induced NAFLD model. Hepatic protein abundance is a function of protein synthesis, degradation and transport into and out of the liver. Epigenetics-related GO processes were enriched in the Aroclor1260 + PCB126 exposure group, and this may have influenced the synthesis rates of specific hepatic proteins. The abundance of multiple epigenetics-related proteins was reduced including histone deacetylase 2; histones H1.2, H1.4, H1.5, and H1t; RNA polymerase-associated protein CTR9 homolog; RNA binding protein 3; and LIM domain-containing protein 1 and protein arginine methyltransferase 7). The proteins are involved in numerous epigenetics processes including histone acetylation, methylation, and microRNAs. IPF demonstrated overconnected interactions with the methyltransferase, PRMT1, and the several transcription factors associated with the epigenetic regulation of gene expression such as ETS1 and GABPα (Sizemore et al. 2017). The abundance of other proteins involved in epigenetics and the regulation of gene expression was altered in the other treatment groups (e.g., the noncanonical poly(A) RNA polymerase PAPD5, Supplementary Table 2) in Aroclor1260). Future studies are required to establish the mechanistic importance of epigenetic mechanisms in the genesis, progression, and potential heritability of PCB-related liver diseases.

Although perhaps the most comprehensive analysis of different chronic PCB exposures in an animal model of NAFLD, the present study is not without its limitations. Most notably, while proteins regulating metal homeostasis and epigenetics were implicated, direct measurement of hepatic metals and epigenetic signatures was not performed. While we previously published a proteomics analyses in the HFD plus Aroclor1260 TASH model (Hardesty et al. 2019b), the present experiment utilized a different, and potentially more sensitive, proteomics technique (TMT labeling) as well as different analytic procedures. This may limit the comparability of results between studies, and as a result, the MetaCore outcomes may vary. Sex differences were previously reported for Aroclor1260-induced TASH (Wahlang et al. 2019c), with female mice being more susceptible. Because male mice were utilized in the present study, potential sex differences for PCB126 and Aroclor1260 + PCB126 exposures in TASH remain unknown. While Aroclor1260 + PCB126 exposures were associated with a pancreatic pathology resembling diabetic exocrine pancreatopathy in an acute model (Hardesty et al. 2019b), the present study did not evaluate pancreatic endpoints because GTT was unchanged.

In conclusion, the present study demonstrated the complexity of the hepatic effects of PCB mixtures. DL PCBs, NDL PCBs, and a more environmentally relevant mixture of both types of PCBs differentially modulated the hepatic proteome and the severity of diet-induced NAFLD. Aroclor1260 increased hepatic inflammation and phosphoprotein signaling disruption consistent with prior research. PCB126 decreased hepatic inflammation and fibrosis at the molecular level. Mechanisms including altered cytoskeletal remodeling, metal homeostasis, and disruption of intermediary and xenobiotic metabolism were implicated in PCB126's mode of action, and all have been previously reported. Neither the histologic nor the proteomic effects of Aroclor1260 and PCB126 were additive in the co-exposure model. PCB126 attenuated Aroclor1260-induced hepatic inflammation but increased hepatic free fatty acids while reducing plasma lipids. The overwhelming majority of differentially regulated hepatic proteins associated with Aroclor1260 + PCB126 exposure were not associated with either Aroclor1260 or PCB1260 exposure. Likewise, most proteins associated with either Aroclor1260 or PCB126 exposures were not associated with co-exposure to both. Despite this, many of the top GO processes and overconnected interactions by protein function were common to the PCB126 and Aroclor1260 + PCB126 exposure groups. These conserved processes were broadly related to metabolism and cellular organization and localization. A complex web of overconnected transcription factors broadly regulating metabolism; liver injury and inflammation; and liver repair was identified. Aroclor1260 + PCB126 exposure was strongly associated with multiple epigenetic processes, and these could potentially explain the observed nonadditive effects of the exposures on the hepatic proteome. When compared with our recently published acute study investigating the same PCB exposures, the modifying effect on diet (and possibly duration) on PCB-induced hepatotoxicity is also demonstrated. More data including translational research are

required on potential modes of PCB action in NAFLD including phosphoprotein signaling disruption; abnormal metal homeostasis; cytoskeletal remodeling; and transcriptional reprogramming by epigenetic mechanisms. Likewise, potential sex differences and the AhR-dependence of PCB126's NAFLD modifying effects warrant future investigation.

Acknowledgements This work was funded, in part, by the National Institutes of Health (R35ES028373 (MCC), P42ES023716 (MCC), T32ES011564 (BW), P20GM113226 (MCC), and P50AA024337 (MCC)). The authors would like to acknowledge: (i) the Omics Core of UofL's Hepatobiology and Toxicology Center, Daniel W. Wilkey and Frederick W. Benz for proteomics assistance; (ii) the Hepatobiology and Toxicology Center's Animal Model and Biorepository Core for the support required to develop and analyze the novel animal exposure models utilized in this manuscript; (iii) the Sample and Data Management Core of UofL's Superfund Research Center; and (iv) Linda S. Birnbaum, PhD, whose idea it was to spike PCB126 into the Aroclor1260 thereby creating a potentially more environmentally relevant PCB mixture for use in experimental studies.

Compliance with ethical standards

Conflict of interest The authors declare that they have no conflict of interest.

Ethical approval All applicable international, national, and/or institutional guidelines for the care and use of animals were followed.

Publisher's note Springer Nature remains neutral with regard to jurisdictional claims in published maps and institutional affiliations.

References

Abera MB, Kazanietz MG (2015) Protein kinase Calpha mediates erlotinib resistance in lung cancer cells. Mol Pharm 87:832–841

Addison RF (1983) PCB replacements in dielectric fluid. Environ Sci Technol 17:486a–494a

Angrish MM, Mets BD, Jones AD, Zacharewski TR (2012) Dietary fat is a lipid source in 2,3,7,8-tetrachlorodibenzo-rho-dioxin (TCDD)-elicited hepatic steatosis in C57BL/6 mice. Toxicol Sci 128:377–386

Bagu ET, Layoun A, Calve A, Santos MM (2013) Friend of GATA and GATA-6 modulate the transcriptional up-regulation of hepcidin in hepatocytes during inflammation. Biometals 26:1051–1065

Bakiri L, Hamacher R, Grana O, Guio-Carrion A, Campos-Olivas R, Martinez L, Dienes HP, Thomsen MK, Hasenfuss SC, Wagner EF (2017) Liver carcinogenesis by FOS-dependent inflammation and cholesterol dysregulation. J Exp Med 214:1387–1409

Bligh EG, Dyer WJ (1959) A rapid method of total lipid extraction and purification. Can J Biochem Physiol 37:911–917

Cave M, Appana S, Patel M, Falkner KC, McClain CJ, Brock G (2010) Polychlorinated biphenyls, lead, and mercury are associated with liver disease in American adults: NHANES 2003-2004. Environ Health Perspect 118:1735–1742

Clair HB, Pinkston CM, Rai SN, Pavuk M, Dutton ND, Brock GN, Prough RA, Falkner KC, McClain CJ, Cave MC (2018) Liver disease in a residential cohort with elevated polychlorinated biphenyl exposures. Toxicol Sci 164:39–49

Ding W, Tan H, Li X, Zhang Y, Fang F, Tian Y, Li J, Pan X (2018) MicroRNA-493 suppresses cell proliferation and invasion by targeting ZFX in human hepatocellular carcinoma. Cancer Biomark 22:427–434

Engholm-Keller K, Larsen MR (2016) Improving the phosphoproteome coverage for limited sample amounts using TiO2-SIMAC-HILIC (TiSH) phosphopeptide enrichment and fractionation. Methods Mol Biol 1355:161–177

Everett CJ, Frithsen I, Player M (2011) Relationship of polychlorinated biphenyls with type 2 diabetes and hypertension. J Environ Monit 13:241–251

Goncharov A, Haase RF, Santiago-Rivera A, Morse G, McCaffrey RJ, Rej R, Carpenter DO (2008) High serum PCBs are associated with elevation of serum lipids and cardiovascular disease in a Native American population. Environ Res 106:226–239

Gonzalez-Teran B, Matesanz N, Nikolic I, Verdugo MA, Sreeramkumar V, Hernandez-Cosido L, Mora A, Crainiciuc G, Saiz ML, Bernardo E, Leiva-Vega L, Rodriguez E, Bondia V, Torres JL, Perez-Sieira S, Ortega L, Cuenda A, Sanchez-Madrid F, Nogueiras R, Hidalgo A, Marcos M, Sabio G (2016) p38gamma and p38delta reprogram liver metabolism by modulating neutrophil infiltration. EMBO J 35:536–552

Hardesty JE, Al-Eryani L, Wahlang B, Falkner KC, Shi H, Jin J, Vivace BJ, Ceresa BP, Prough RA, Cave MC (2018) Epidermal growth factor receptor signaling disruption by endocrine and metabolic disrupting chemicals. Toxicol Sci 162:622–634

Hardesty JE, Wahlang B, Falkner KC, Clair HB, Clark BJ, Ceresa BP, Prough RA, Cave MC (2017) Polychlorinated biphenyls disrupt hepatic epidermal growth factor receptor signaling. Xenobiotica 47:807–820

Hardesty JE, Wahlang B, Falkner KC, Shi H, Jin J, Wilkey D, Merchant M, Watson C, Prough RA, Cave MC (2019a) Hepatic signalling disruption by pollutant Polychlorinated biphenyls in steatohepatitis. Cell Signal 53:132–139

Hardesty JE, Wahlang B, Falkner KC, Shi H, Jin J, Zhou Y, Wilkey DW, Merchant ML, Watson CT, Feng W, Morris AJ, Hennig B, Prough RA, Cave MC (2019b) Proteomic analysis reveals novel mechanisms by which polychlorinated biphenyls compromise the liver promoting diet-induced steatohepatitis. J Proteome Res 18:1582–1594

Heindel JJ, Blumberg B, Cave M, Machtinger R, Mantovani A, Mendez MA, Nadal A, Palanza P, Panzica G, Sargis R, Vandenberg LN, Vom Saal F (2017) Metabolism disrupting chemicals and metabolic disorders. Reprod Toxicol 68:3–33

Jan YH, Lai TC, Yang CJ, Huang MS, Hsiao M (2019) A co-expressed gene status of adenylate kinase 1/4 reveals prognostic gene signature associated with prognosis and sensitivity to EGFR targeted therapy in lung adenocarcinoma. Sci Rep 9:12329

Keshishian H, Burgess MW, Gillette MA, Mertins P, Clauser KR, Mani DR, Kuhn EW, Farrell LA, Gerszten RE, Carr SA (2015) Multiplexed, quantitative workflow for sensitive biomarker discovery in plasma yields novel candidates for early myocardial injury. Mol Cell Proteom 14:2375–2393

Klaren WD, Gadupudi GS, Wels B, Simmons DL, Olivier AK, Robertson LW (2015) Progression of micronutrient alteration and hepatotoxicity following acute PCB126 exposure. Toxicology 338:1–7

Klaren WD, Vine D, Vogt S, Robertson LW (2018) Spatial distribution of metals within the liver acinus and their perturbation by PCB126. Environ Sci Pollut Res Int 25:16427–16433

Koh MY, Gagea M, Sargis T, Lemos Jr. R, Grandjean G, Charbono A, Bekiaris V, Sedy J, Kiriakova G, Liu X, Roberts LR, Ware C, Powis G (2016) A new HIF-1alpha/RANTES-driven pathway to hepatocellular carcinoma mediated by germline haploinsufficiency of SART1/HAF in mice. Hepatology 63:1576–1591

Lei CT, Wei YH, Tang H, Wen Q, Ye C, Zhang C, Su H (2017) PKC-alpha triggers EGFR ubiquitination, endocytosis and ERK

activation in podocytes stimulated with high glucose. Cell Physiol Biochem 42:281–294
Marcher AB, Bendixen SM, Terkelsen MK, Hohmann SS, Hansen MH, Larsen BD, Mandrup S, Dimke H, Detlefsen S, Ravnskjaer K (2019) Transcriptional regulation of hepatic stellate cell activation in NASH. Sci Rep 9:2324
McDowell GS, Gaun A, Steen H (2013) iFASP: combining isobaric mass tagging with filter-aided sample preparation. J Proteome Res 12:3809–3812
Merino-Azpitarte M, Lozano E, Perugorria MJ, Esparza-Baquer A, Erice O, Santos-Laso A, O'Rourke CJ, Andersen JB, Jimenez-Aguero R, Lacasta A, D'Amato M, Briz O, Jalan-Sakrikar N, Huebert RC, Thelen KM, Gradilone SA, Aransay AM, Lavin JL, Fernandez-Barrena MG, Matheu A, Marzioni M, Gores GJ, Bujanda L, Marin JJG, Banales JM (2017) SOX17 regulates cholangiocyte differentiation and acts as a tumor suppressor in cholangiocarcinoma. J Hepatol 67:72–83
Niopek K, Ustunel BE, Seitz S, Sakurai M, Zota A, Mattijssen F, Wang X, Sijmonsma T, Feuchter Y, Gail AM, Leuchs B, Niopek D, Staufer O, Brune M, Sticht C, Gretz N, Muller-Decker K, Hammes HP, Nawroth P, Fleming T, Conkright MD, Bluher M, Zeigerer A, Herzig S, Berriel Diaz M (2017) A hepatic GAbp-AMPK axis links inflammatory signaling to systemic vascular damage. Cell Rep 20:1422–1434
Patandin S, Koopman-Esseboom C, de Ridder MA, Weisglas-Kuperus N, Sauer PJ (1998) Effects of environmental exposure to polychlorinated biphenyls and dioxins on birth size and growth in Dutch children. Pediatr Res 44:538–545
Qin XY, Suzuki H, Honda M, Okada H, Kaneko S, Inoue I, Ebisui E, Hashimoto K, Carninci P, Kanki K, Tatsukawa H, Ishibashi N, Masaki T, Matsuura T, Kagechika H, Toriguchi K, Hatano E, Shirakami Y, Shiota G, Shimizu M, Moriwaki H, Kojima S (2018) Prevention of hepatocellular carcinoma by targeting MYCN-positive liver cancer stem cells with acyclic retinoid. Proc Natl Acad Sci USA 115:4969–4974
Raffetti E, Donato F, Speziani F, Scarcella C, Gaia A, Magoni M (2018) Polychlorinated biphenyls (PCBs) exposure and cardiovascular, endocrine and metabolic diseases: a population-based cohort study in a North Italian highly polluted area. Environ Int 120:215–222
Rommelaere S, Millet V, Vu Manh TP, Gensollen T, Andreoletti P, Cherkaoui-Malki M, Bourges C, Escaliere B, Du X, Xia Y, Imbert J, Beutler B, Kanai Y, Malissen B, Malissen M, Tailleux A, Staels B, Galland F, Naquet P (2014) Sox17 regulates liver lipid metabolism and adaptation to fasting. PLoS ONE 9:e104925
Rosenbaum PF, Weinstock RS, Silverstone AE, Sjodin A, Pavuk M (2017) Metabolic syndrome is associated with exposure to organochlorine pesticides in Anniston, AL, United States. Environ Int 108:11–21
Safe S, Bandiera S, Sawyer T, Robertson L, Safe L, Parkinson A, Thomas PE, Ryan DE, Reik LM, Levin W (1985) PCBs: structure-function relationships and mechanism of action. Environ Health Perspect 60:47–56
Serdar B, LeBlanc WG, Norris JM, Dickinson LM (2014) Potential effects of polychlorinated biphenyls (PCBs) and selected organochlorine pesticides (OCPs) on immune cells and blood biochemistry measures: a cross-sectional assessment of the NHANES 2003-2004 data. Environ Health 13:114
Shepard BD, Tuma PL (2010) Alcohol-induced alterations of the hepatocyte cytoskeleton. World J Gastroenterol 16:1358–1365
Shi H, Jan J, Hardesty JE, Falkner KC, Prough RA, Balamurugan AN, Mokshagundam SP, Chari ST, Cave MC (2019) Polychlorinated biphenyl exposures differentially regulate hepatic metabolism and pancreatic function: implications for nonalcoholic steatohepatitis and diabetes. Toxicol Appl Pharmacol 363:22–33
Silverstone AE, Rosenbaum PF, Weinstock RS, Bartell SM, Foushee HR, Shelton C, Pavuk M (2012) Polychlorinated biphenyl (PCB) exposure and diabetes: results from the Anniston Community Health Survey. Environ health Perspect 120:727–732
Sizemore GM, Pitarresi JR, Balakrishnan S, Ostrowski MC (2017) The ETS family of oncogenic transcription factors in solid tumours. Nat Rev Cancer 17:337–351
Srivastava S (2019a) Designing and sample size calculation in presence of heterogeneity in biological studies involving high-throughput data. Electronic Theses and Dissertations. Paper 3261. https://doi.org/10.18297/etd/3261
Srivastava S, Merchant M, Rai A, Rai SN (2019b) Interactive web tool for standardizing proteomics workflow for liquid chromatography-mass spectrometry data. J Proteom Bioinform 12:85–88
Srivastava S, Merchant M, Rai A, Rai SN (2019c) Standardizing proteomics workflow for liquid chromatography-mass spectrometry: technical and statistical considerations. J Proteom Bioinform 12:48–55
ten Tusscher GW, Steerenberg PA, van Loveren H, Vos JG, von dem Borne AE, Westra M, van der Slikke JW, Olie K, Pluim HJ, Koppe JG (2003) Persistent hematologic and immunologic disturbances in 8-year-old Dutch children associated with perinatal dioxin exposure. Environ Health Perspect 111:1519–1523
Wahlang B, Barney J, Thompson B, Wang C, Hamad OM, Hoffman JB, Petriello MC, Morris AJ, Hennig B (2017a) Editor's Highlight: PCB126 Exposure Increases Risk for Peripheral Vascular Diseases in a Liver Injury Mouse Model. Toxicological sciences: an official journal of the Society of Toxicology 160:256–267
Wahlang B, Falkner KC, Clair HB, Al-Eryani L, Prough RA, States JC, Coslo DM, Omiecinski CJ, Cave MC (2014a) Human receptor activation by aroclor 1260, a polychlorinated biphenyl mixture. Toxicol Sci 140:283–297
Wahlang B, Hardesty JE, Jin J, Falkner KC, Cave MC (2019a) Polychlorinated biphenyls in nonalcoholic fatty liver diseae. Curr Opin Toxicol 14:21–28
Wahlang B, Jin J, Beier JI, Hardesty JE, Daly EF, Schnegelberger RD, Falkner KC, Prough RA, Kirpich IA, Cave MC (2019b) Mechanisms of environmental contributions to fatty liver disease. Curr Environ Health Rep 6:80–94
Wahlang B, Jin J, Hardesty JE, Head KZ, Shi H, Falkner KC, Prough RA, Klinge CM, Cave MC (2019c) Identifying sex differences arising from polychlorinated biphenyl exposures in toxicant-associated liver disease. Food Chem Toxicol 129:64–76
Wahlang B, Perkins JT, Petriello MC, Hoffman JB, Stromberg AJ, Hennig B (2017b) A compromised liver alters polychlorinated biphenyl-mediated toxicity. Toxicology 380:11–22
Wahlang B, Prough RA, Falkner KC, Hardesty JE, Song M, Clair HB, Clark BJ, States JC, Arteel GE, Cave MC (2016) Polychlorinated biphenyl-xenobiotic nuclear receptor interactions regulate energy metabolism, behavior, and inflammation in non-alcoholic-steatohepatitis. Toxicol Sci 149:396–410
Wahlang B, Song M, Beier JI, Cameron Falkner K, Al-Eryani L, Clair HB, Prough RA, Osborne TS, Malarkey DE, Christopher States J, Cave MC (2014b) Evaluation of Aroclor 1260 exposure in a mouse model of diet-induced obesity and non-alcoholic fatty liver disease. Toxicol Appl Pharmacol 279:380–390
Wisniewski JR, Zougman A, Nagaraj N, Mann M (2009) Universal sample preparation method for proteome analysis. Nat Methods 6:359–362
Yin N, Lepp A, Ji Y, Mortensen M, Hou S, Qi XM, Myers CR, Chen G (2017) The K-Ras effector p38gamma MAPK confers intrinsic resistance to tyrosine kinase inhibitors by stimulating EGFR

transcription and EGFR dephosphorylation. J Biol Chem 292:15070–15079

Zhao J, O'Neil M, Vittal A, Weinman SA, Tikhanovich I (2019) PRMT1-dependent macrophage IL-6 production is required for alcohol-induced HCC progression. Gene Expr 19:137–150

Zhou L, Tang J, Yang X, Dong H, Xiong X, Huang J, Zhang L, Qin H, Yan S (2019) Five constituents in *Psoralea corylifolia* L. Attenuate palmitic acid-induced hepatocyte injury via inhibiting the protein kinase C-alpha/nicotinamide-adenine dinucleotide phosphate oxidase pathway. Front Pharm 10:1589